FE-SIMULATIONS OF RAPID SILO FLOW WITH A POLAR ELASTO-PLASTIC CONSTITUTIVE MODEL

JACEK TEJCHMAN

Institute for Concrete Structures,
Technical University of Gdansk
Narutowicza 11/12, 80-952 Gdansk-Wrzeszcz, Poland

Abstract: The paper presents results on numerical modelling of rapid flow of granular materials in a model silo with convergent smooth walls. The calculations were performed with a finite element method based on a polar elasto-plastic constitutive relation by Mühlhaus. The relation differs from the conventional theory of plasticity by the presence of Cosserat rotations and couple stresses using a mean grain diameter as a characteristic length. The characteristic length causes that numerical results do not depend upon the mesh discretisation. The model tests on rapid silo flow of glass beads performed by Renner in a glass hopper with a large wall inclination from the bottom were numerically simulated. The plane strain FE-calculations were performed by taking into account inertial forces and linear viscous damping. A satisfactory agreement between numerical and experimental results was obtained. Advantages and limitations of a continuum approach for simulations of rapid silo flow were outlined.

1. Introduction

The existing theoretical models on silo flow of granular materials can be divided into models treating the silo fill as continuum and as separate particles. The first models based mainly on a finite element method are more suitable for slow silo flow, i.e. flow with low deformation rates, where the particles behave as a conglomerate and exhibit solidlike behaviour. During such flow, the internal stresses are generated only by normal and friction forces between particles. The second models using granular dynamics algorithms, kinetic theories or cellular automata approaches correspond to rapid silo flow where the material behaves like gas or dense fluid. Rapid flow is connected to high deformation rates and large inertial forces. During such flow, the particles loose oft their contacts and are subject to short impulsive collisions and overriding. The internal stresses are due to normal and friction forces between grains and collisions. Slow and rapid flow are dissipative. For slow flow, energy is slightly lost due to friction as grains slide across each other. For rapid flow, energy is strongly lost because particle collisions are inherently inelastic. Both types of flow may occur simultaneously at different locations in a silo. Usually, material at the outlet is in the rapid flow regime and the material higher up is moving slowly.

The intention of the theoretical research presented in this paper is to study the onset of rapid flow of granular material in a plane strain model hopper with a large wall inclination from the bottom. The study was performed with a continuum model based on a finite element method and taking into account a polar elasto-plastic constitutive law. The used model is a continuum approach but it has some properties characteristic for discrete models. It includes, namely, a mean grain diameter, grain rotations and couple stresses. To describe the material dynamics and the possibility of energy loss during grain collisions in rapid flow, inertial forces and viscous damping were also included. The FE-results were compared with corresponding model tests carried out on glass beads flowing in a glass hopper with a large wall inclination from the bottom. The used approach turned to be realistic for description of usual silo flow (Tejchman 1995, 1996, 1997) but it has not been verified for extremely rapid flow yet which takes place in hoppers with a large wall inclination (rather unusual in the silos practice).

The available analytical continuum theories of stress analysis in silos are too simple and not sufficient to realistically describe the material behaviour during dynamic flow. They were derived from quasi-static assumptions without taking into account the deformations in silo fill and inertial effects. Some of these methods were formulated by classical methods of plasticity (Walker 1967, Walters 1973, Horn and Nedderman 1976, Drescher 1983) assuming a total plastification of the fill in the silo which does not take place in reality. Other formulae were based upon assumptions (elastic stress field by Fröhlich 1934, active and passive stress state by Airy 1987, associated flow rule by Mróz and Drescher 1968, Mróz and Szymański 1971, radial stress field by Jenike 1964, circular distribution of the major principle stresses by Enstad 1975, and static and kinematic bounds theorems by Melix 1985) which were not verified by experiments. In addition, the assumption in most silo theories of a constant wall friction angle (to be determined with wall shear tests) as boundary condition along the wall is not realistic because the wall friction angle changes during shearing and depends on the boundary conditions of the entire system (Tejchman 1989). The existing FEM-solutions of silo flow by Häußler and Eibl (1984), Eibl and Rombach (1988), Vedaie and Bishara (1988), Tano et al. (1994), Ragneau and Areibert (1995), Ruckenbrod and Eibl (1995) are more realistic than analytical silo formulae. Their big advantage is the possibility to consider large systems. However, they were obtained within a non-polar elasto-plastic continuum and thus, the results were dependent on the magnitude of the element mesh. Moreover, some of them did not consider the material softening due to the shear zone formation, and others inertial forces. They were also unable to consistently describe the interface behaviour along the silo wall. The influence of wall roughness and cohesion on flow was not investigated too. Due to an assumption of large viscous damping (Häußler and Eibl 1984, Eibl and Rombach 1988), the calculated stresses during silo emptying had a quasi-static character. The dynamic pulsations in a silo fill during flow (Ruckenbrod and Eibl 1995) were obtained under a doubtful assumption of a decrease of the wall friction coefficient in the region of high flow velocities.

Tejchman (1989, 1997), Gudehus and Tejchman (1991) showed that many mechanisms of granular mass in silos at the onset of quasi-static mass flow with controlled outlet velocity (formation of shear zones, interaction between the wall with variable roughness and the silo fill, stress fluctuations, grain size effects) could realistically be described with a polar elasto-plastic and polar hypoplastic approach. The numerical results were independent of the mesh size. The polar boundary conditions on the wall proved to be more realistic than the classical ones. Using the same approaches with an additional consideration of inertial forces, Tejchman and Gudehus (1993) and Tejchman (1995, 1997) successfully described silo the onset of dynamic flow with controlled and free outlet velocity.

The granular dynamics algorithms (Cundall and Strack 1979, Walton and Braun 1986, Savage 1992, Sakaguchi and Ozaki 1993, Thornton and Sun 1993) are powerful research techniques for giving insight into flow behaviour at the microscopic level since they handle particle properties directly. The calculated flow patterns in model silos with these algorithms are consistent with experimental work, but the calculated stresses in the silo fill are only qualitatively in agreement with measured ones (Kafui and Thornton 1995, 1997, Langston et al. 1995, Gutfraind and Pouliquen 1995, Pouliquen and Gutfraind 1996, Lin et al. 1996, Masson et al. 1996, Luding et al. 1996, Ristow 1997). This is so as the determination of both micro-structural material parameters and wall boundary conditions is difficult. There is simply no experimental data on micro-structural parameters which could help to calibrate better the granular dynamics models. At present, these models demand too much computer time and thus they are not relevant for large silos. They certainly belong to future methods on investigation of flow behaviour in silos since they follow the motion of all particles and their interactions at each time step in detail. Their availability grows with the appearance of more and more powerful computers.

An alternative to the use of granular-dynamics computer simulations to predict the rapid granular flow behaviour are analytical kinetic theories (Savage and Jeffrey 1981, Haff 1983, Jenkins and Richman 1985, Lun and Savage 1987, Jenkins 1992) which were developed in terms of analogies to the flow of gases and dense fluids at the molecular level, i.e. in terms of a molecular chaos without long duration contacts. In order to account for the velocity fluctuations, the concept of granular temperature was introduced. Fütterer (1991) used a model by Haff (1983) to describe the material behaviour during rapid flow in converging canals. Only qualitative agreement with experimental data was achieved. As in the case of molecular dynamics algorithms, the identification of material constants and the assumption of realistic wall boundary conditions was not possible.

Cellular automata approaches (Baxter and Behringer 1990, Martinez et al. 1995), which describe the material flow as an upward propagation and diffusion of holes through the lattice, are purely kinematic models and no flow dynamics is involved. Thus, they are not apt to realistically model silo flow.

The paper is organised as follows. At the beginning some results of model silo tests on rapid flow in a model hopper are shown. Next, a plane polar continuum is

briefly presented. Later, a polar elasto-plastic constitutive law is summarised which is used for investigations of rapid flow. The polar boundary conditions and the FE-implementation are presented as well. Then, the FE-results for plane strain flow are depicted. Finally, the conclusions from numerical analyses are discussed.

2. Model Tests

Model tests on rapid silo flow were performed in a flat silo model with convergent glass walls (Buggish and Renner 1993, Renner 1996). The model was 0.9 m high and 0.02-0.045 m thick. The wall inclination from the bottom was $\alpha = 82^{\circ}$-87.5°, the width at the bottom $b_1 = 0.02$-0.08 m, and the width at the top $b_2 = 0.13$ m. As the fills, the dry glass beads with two different mean diameters were used, viz. $d_{50} = 2.3$ mm and 4.5 mm. The flow of the fill out of the hopper was gravitational. Due to a large wall inclination from the bottom, the flow was rapid. The wall shear stress and wall normal stress were measured with a transducer placed at half of the height of one wall. The transducer consisted of one vertical and one horizontal beam. The stresses were obtained with the aid of strain gauges which were stuck to the beams. The displacements of glass particles during flow were registered with a high speed video-camera which was apt to make 1000 photographs in 1s. In addition, air pressure inside the silo fill was measured.

Fig.2.1 shows typical recorded signals of the normal (n and shear stress (w at the mid-point of the glass wall during filling, storing and flow ($\alpha = 87.5^{\circ}$, $b_1 = 0.04$ m,

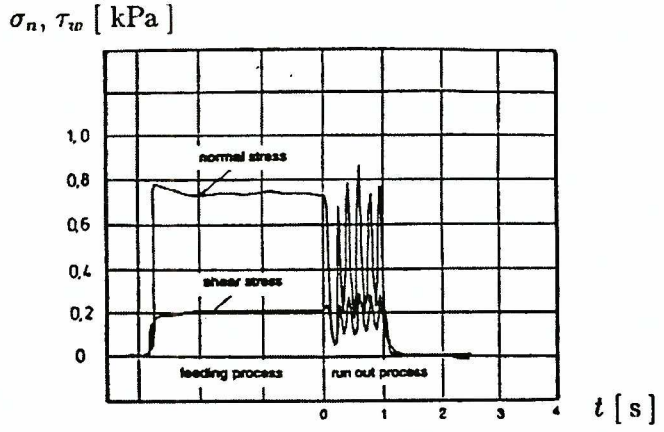

Figure.2.1. Measured shear τ_w and normal σ_n stress on the wall during rapid flow (Renner 1996)

$d_{50} = 2.3$ mm). During flow, the wall stresses pulsate strongly about their mean values with a frequency of about $f = 5.5$ Hz. The pulsations are almost harmonic. The amplitude from peak to peak of the normal wall stress is about 0.6 kPa and of the shear wall stress 0.2 kPa. The normal wall stress pulsates around the mean value of 0.5 kPa, and the shear wall stress around 0.2 kPa. The mean wall friction angle is found to be almost constant, i.e. $\bar{\varphi}_w = \arctan(\tau_w/\sigma_n) = 18.4^{\circ}$. The pulsations

are caused by disturbances of the material flow at the silo outlet. The disturbances propagate through the fill in the form of longitudinal stress waves opposite to the flow direction. The velocity of these stress waves, $v_c = 2.7$ m/s, was estimated on the basis of the measured velocities of neighbouring particles, and was approximately nine times as large as the mean flow velocity, $v_f = 0.3$ m/s. The value of v_f was approximately equal to a theoretical value for the mean flow velocity at the silo outlet given by the experimental formula by Schwedes (1968):

$$v_v = 0.5\sqrt{g b_o} = 0.5\sqrt{9.81 \cdot 0.04} = 0.3 \text{ m/s}, \tag{2.1}$$

wherein b_o is the outlet width and g denotes the gravitational acceleration. The measured velocity and frequency of stress waves in the fill during rapid flow are significantly smaller than the velocity and frequency of longitudinal stress waves propagating through a compact granular body. During rapid flow in the hopper, numerous hollow spaces were observed in the fill which strongly reduced the velocity and frequency of propagating stress waves. The more compact the granular body, the higher the wave velocity and frequency. The slower the flow, the more compact the bulk solid remains. The velocity and frequency of waves during rapid flow in silos with smooth walls cannot be simply estimated from the formula for wave propagation in an elastic bar of a silo height (Tejchman 1997) because the propagation way and the modulus of elasticity are different due to the occurrence of hollow spaces in the flowing material.

In addition, the model tests by Renner (1996) revealed that the mean stresses increased with increasing wall inclination α. The velocity v_c and frequency f of stress waves increased almost linearly with decreasing α. The influence of b_1 on the results was insignificant.

3. Plane Polar Continuum

A rectangular (x_1, x_2) coordinate system is used, where x_i are the coordinates of material points in the actual configuration. A polar (Cosserat) continuum differs from a classical (non-polar) continuum in that an additional rotation (called ω^c) appears in the kinematics (Günther 1958, Schäfer 1962, Mindlin 1964). Thus, each material point of the polar continuum has three degrees of freedom: two translational degrees of freedom, namely u_1 and u_2, and one rotational degree of freedom ω^c (Fig.3.1). During deformation, the material points are displaced by u_1 and u_2, and at the same time are rotated from their initial positions by an angle ω^c with respect to the axes of x_1 and x_2. The rotation takes place around the rotation axis x_3 which is orthogonal to the 1,2-plane. ω^c, which originates from the micro-rotation of the micro-elements in a polar continuum, is independent of the displacements in contrast to the rotation in a non-polar continuum:

$$\omega_{ij} = 0.5(u_{i,j} - u_{j,i}). \tag{3.1}$$

The state of deformation within a polar continuum is described by the following six deformation quantities (which are considered here as infinitesimal):

$$\varepsilon_{11} = u_{1,1}\,,\ \varepsilon_{22} = u_{2,2}\,, \tag{3.2}$$

$$\varepsilon_{12} = u_{1,2} + \omega^c\,,\ \varepsilon_{21} = u_{2,1} - \omega^c\,, \tag{3.3}$$

$$\kappa_1 = \omega^c_{,1}\,,\ \kappa_2 = \omega^c_{,2}\,, \tag{3.4}$$

where

$$()_{,i} = \partial()/\partial x_i\,. \tag{3.5}$$

ε_{ij} are components of the deformation tensor and κ_i are components of the curvature vector. The normal deformations are defined similar as in a non-polar continuum. The shear deformations ε_{12} and ε_{21} can be viewed as a relative deformation relating the macro-displacement gradient and the micro-rotation

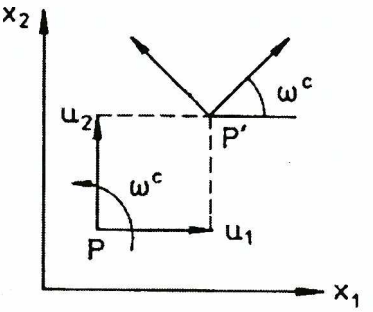

Figure 3.1. *Degrees of freedom in a plane Cosserat continuum: u_1, u_2 — horizontal and vertical displacement, ω^c — Cosserat rotation, P — material point*

(Fig.3.2); in contrast to a non-polar continuum $\varepsilon_{12} \neq \varepsilon_{21}$. The curvatures κ_1 and κ_2 describe the macro-deformation gradients of the micro-rotation (Fig.3.2). ε_{ij} and κ_i are invariant with respect to rigid body motions (Günther 1958, Mühlhaus 1989). The deformation tensor ε_{ij} can be decomposed into a symmteric part E_{ij} and a skew symmetric part W_{ij}–W^c_{ij}:

$$\varepsilon_{ij} = E_{ij} + W_{ij} - W^c_{ij}\,, \tag{3.6}$$

where

$$E_{ij} = 0.5(u_{i,j} + u_{j,i})\,, \tag{3.7}$$

$$W_{ij} = \omega_{ij} = 0.5(u_{i,j} - u_{j,i})\,, \tag{3.8}$$

$$W^c_{11} = W^c_{22} = 0\,,\ W^c_{12} = -W^c_{21} = -\omega^c\,. \tag{3.9}$$

E_{ij} and W_{ij} denote the symmetric and the skew symmetric part of the displacement gradient, respectively, and W^c_{ij} denotes the skew symmetric tensor corresponding to the Cosserat rotation ω^c. E_{ij} is the deformation tensor and W_{ij} is the rotation tensor which are characteristic of a non-polar continuum. The skew symmetric part

$W_{ij} - W_{ij}^c$ designates the difference between the macro- and the micro-rotation. If $W_{ij} = W_{ij}^c$, ε_{ij} reduces to E_{ij} and the kinematics of a non-polar continuum is retrieved. If $W_{ij} < W_{ij}^c$, an overall negative (clockwise) Cosserat rotation emerges.

The conditions for the compatibility of deformations and curvatures are (Günther 1958):

$$\varepsilon_{11,2} - \varepsilon_{12,1} + \kappa_1 = 0, \tag{3.10}$$

$$\varepsilon_{22,1} - \varepsilon_{21,2} + \kappa_2 = 0, \tag{3.11}$$

$$\kappa_{1,2} - \kappa_{2,1} = 0. \tag{3.12}$$

Six deformation quantities are conjugate with respect to energy to six stress quantities referred to the actual configuration. Four components of ε_{ij} are associated with four components of the stress tensor σ_{ij} which is in general non-symmetric ($\sigma_{12} \neq \sigma_{21}$). The curvatures κ_i are associated with the couple stresses m_i. Fig.3.3 shows the stresses, the couple stresses, the volume body forces f_i^B, the volume body moment m^B, the volume inertia forces $\rho\ddot{u}_i$, and the volume moment of spin inertia $\theta\ddot{\omega}^c$ at an infinitesimal element (dx_1, dx_2) of a plane Cosserat continuum. Force equilibrium and moment equilibrium give the following equations of motion

$$\sigma_{11,1} + \sigma_{12,2} - f_1^B + \rho\ddot{u}_1 = 0, \tag{3.13}$$

$$\sigma_{21,1} + \sigma_{22,2} - f_2^B + \rho\ddot{u}_2 = 0, \tag{3.14}$$

$$m_{1,1} + m_{2,2} + \sigma_{21} - \sigma_{12} - m^B + \theta\ddot{\omega}^c = 0, \tag{3.15}$$

where

$$\ddot{()} = d^2()/dt^2 \tag{3.16}$$

ρ is the mass density and θ is the volume moment of inertia.

The representation of stresses in the Mohr plane leads to a circle whose centre is displaced along the shear ordinate. The coordinates of the centre σ_c and τ_c are:

$$\sigma_c = 0.5(\sigma_{11} + \sigma_{22}), \ \tau_c = 0.5(\sigma_{12} - \sigma_{21}), \tag{3.17}$$

and the circle's radius r is:

$$r^2 = 0.25(\sigma_{11} - \sigma_{22})^2 + 0.25(\sigma_{12} + \sigma_{21})^2 \tag{3.18}$$

The principle stresses σ_1 and σ_2 are expressed by the relation:

$$\sigma_{1/2} = 0.5(\sigma_{11} + \sigma_{22}) \pm \sqrt{0.25(\sigma_{11} - \sigma_{22})^2 + 0.25(\sigma_{12} + \sigma_{21})^2} \tag{3.19}$$

The equilibrium conditions (Eqs.3.13–3.15) are equivalent to the virtual work principle:

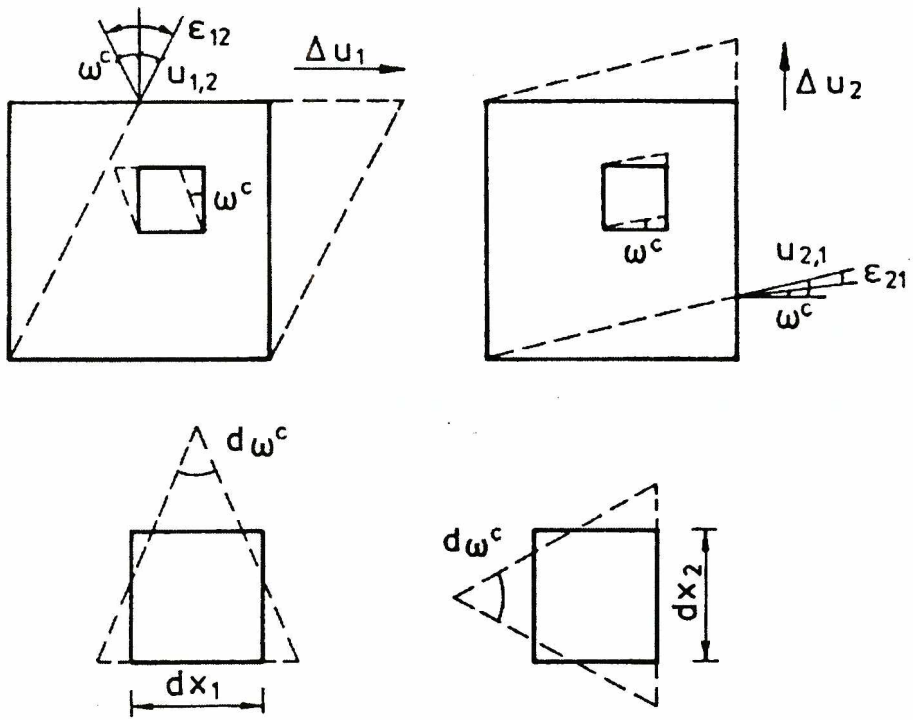

Figure 3.2. Shear deformations ε_{12}, ε_{21} and curvatures κ_1, κ_2 in a plane Cosserat continuum

$$\int_B (\sigma_{ij}\delta\varepsilon_{ij} + m_i\delta\kappa_i)dV = \int_B [(f_i^B - \rho\ddot{u}_i)\delta u_i + (m^B - \theta\ddot{\omega}^c)\delta\omega^c]dV +$$

$$+ \int_{\partial_1 B} t_i\delta u_i dA + \int_{\partial_2 B} m\delta\omega^c dA, \tag{3.20}$$

where

$$\sigma_{ij}\, n_j = t_i \quad \text{on} \quad \partial_1 \mathrm{B}, \qquad n_i n_i = m \quad \text{on} \quad \partial_2 \mathrm{B}. \tag{3.21}$$

t_i and m are prescribed boundary tractions and moment, respectively, $\delta\varepsilon_{ij}$ and $\delta\kappa_i$ denote the virtual deformations and curvatures, δu_i is the virtual displacement, $\delta\omega^c$ is the virtual Cosserat rotation and V is the body volume. The virtual displacements and virtual Cosserat rotations vanish on those parts of the boundary where kinematic boundary conditions are prescribed. The work principle states that the fields σ_{ij}, mi satisfying for arbitrary kinematically admissible virtual δu_i, $\delta\omega^c$ also satisfy the equilibrium conditions (Eqs.3.13-3.15) and the boundary

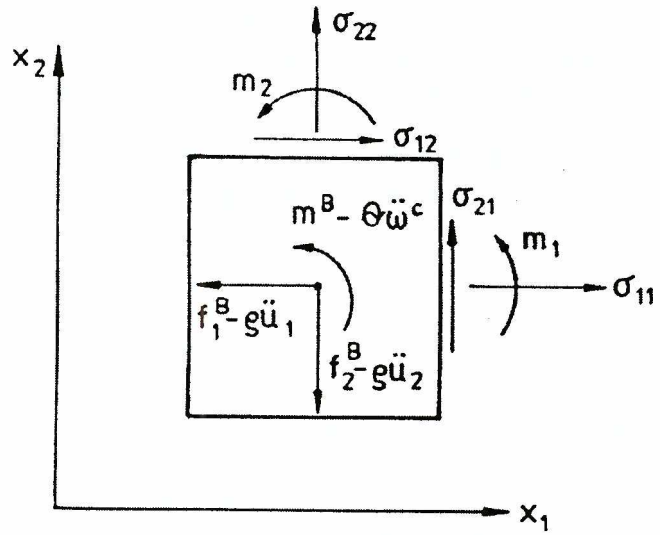

Figure 3.3. Stresses σ_{ij} and couple stresses m_i, volume loads f_i^B and m^B, and volume inertia loads $\rho \ddot{u}_i$ and $\theta\ddot{\omega}^c$ at at an element of a plane Cosserat continuum

conditions (Eqs.3.21). The virtual work principle is used to formulate a FEM of motion (Tejchman 1989). As a consequence of the presence of rotations and couple stresses, the constitutive law for granular materials within a polar continuum is endowed with a characteristic length corresponding to a mean grain diameter (Mühlhaus 1989). Thus, the numerical results are independent of the spatial discretisation (Tejchman 1989, 1994, 1997, Sluys 1992) and boundary value problems remain mathematically well-posed (Benallal et al. 1991, de Borst et al. 1992, Sluys 1992). Due to the presence of a characteristic length, a polar approach can model the thickness of shear zones and related grain size scale effects (Tejchman 1997). Otherwise, numerical results produce unreliable results. Shear zones become narrower upon mesh refinement and computed load-displacements curves change considerably (Tejchman 1989). A polar approach is more suitable to model shear zones in granulates as compared to other models able to capture localisation of deformations in a proper manner (e.g. non-local, strain gradient and viscous models, Sluys 1992) on better physical grounds since it takes into account rotations and couple stresses which are observed during shearing (Oda et al. 1982, Uesugi 1987, Uesugi et al. 1988, Oda 1993) but remain negligible during homogeneous deformation. A polar model is stiffer and stronger than a non-polar one because the work of a Cosserat continuum (Eq.3.20) is augmented by couple stresses, curvatures and rotations which depend upon the mean grain size. Thus, the additional degree of freedom of a polar continuum releases the additional resistance against itself. The FE-calculations show that the thickness of shear zones does not depend upon the mesh refinement if the size of finite elements in the shear zone is not greater than five times the mean grain

diameter when using triangular finite elements with linear shape functions for displacements and a Cosserat rotation (Tejchman 1989, 1997).

For detailed treatment of a polar continuum, the reader is referred to Günther (1958), Schäfer (1962), Mindlin (1964) and Mühlhaus (1987, 1989, 1990).

4. Polar Elasto-Plastic Constitutive Relation for Granulates

Bogdanova-Bontscheva and Lippmann (1975) showed for the first time that Cosserat type rotations appear during shearing of granular materials. The couple stresses were found to be insignificant. Further studies by Becker and Lippmann (1977) and Kanatani (1979) showed that the Cosserat effects are of major importance only along the boundaries. A Cosserat elasto-plastic constitutive model for granular materials with isotropic hardening and softening was proposed by Mühlhaus (1987) and further developed by Mühlhaus und Vardoulakis (1987) and Mühlhaus (1988, 1990). It differs from the conventional theory of plasticity by the presence of Cosserat rotations and couple stresses using the mean grain diameter as a characteristic length. It can be summarised as follows:

$$\dot{\varepsilon}_{ij} = \dot{\varepsilon}^{e}_{ij} + \dot{\varepsilon}^{p}_{ij}, \quad \dot{\kappa}_i = \dot{\kappa}^{e}_{i} + \dot{\kappa}^{p}_{i}, \tag{4.1}$$

$$\dot{\varepsilon}^{e}_{ij} = \frac{1}{E}[(1+\nu)\dot{\sigma}_{ij} - \nu\dot{\sigma}_{kk}], \; i = k, \tag{4.2}$$

$$\dot{\varepsilon}^{e}_{ij} = \frac{1}{2G}\frac{\partial \dot{\tau}^{2}}{\partial \sigma_{ij}}, \quad \dot{\kappa}^{e}_{i} = \frac{1}{2G}\frac{\partial \dot{\tau}^{2}}{\partial m_i}, \; i \neq j, \tag{4.3}$$

$$\dot{\varepsilon}^{p}_{ij} = \lambda\frac{\partial g}{\partial \sigma_{ij}}, \quad \dot{\kappa}^{p}_{i} = \lambda\frac{\partial g}{\partial m_i}, \tag{4.4}$$

$$\tau = (a_1 s_{ij}s_{ij} + a_2 s_{ij}s_{ji} + \frac{a_3}{d_{50}^2} m_i m_i)^{0.5}, \tag{4.5}$$

$$f = \tau + \mu(e_0, \gamma^p)p, \tag{4.6}$$

$$g = \tau + \alpha(e_0, \gamma^p)p, \tag{4.7}$$

wherein τ is the second invariant of the deviatoric stress tensor, s_{ij} — non-symmetric deviatoric stress tensor ($s_{ij} = \sigma_{ij} - p\delta_{ij}$) p — mean stress, σ_{ij} — stress tensor, m_i — couple stress vector, $a_1 = 3/8$, $a_2 = 1/8$, $a_3 = 1$ — coefficients, d_{50} mean grain diameter, f — yield function, g — potential function, μ — mobilised friction factor, α — mobilised dilatancy factor, e_0 — initial void ratio, γ^p — plastic shear deformation, ε_{ij} — deformation tensor, $\dot{\varepsilon}_{ij}$ — rate of deformation tensor,

κ_i — curvature vector, $\dot{\kappa}_i$ — rate of curvature vector, λ — proportionality factor, E — elastic modulus, G — shear modulus, ν — Poisson ratio, δ_{ij} — Kronecker delta. The superimposed indexes e and p designate the elastic and the plastic strain or curvature, respectively. The meaning of f, g, τ, γ^p and λ is analogous to non-polar plasticity (Mróz 1963). In the τ, p-plane, the equations $f = 0$ and $g = 0$ describe a yield and a flow potential curve (Fig.4.1). The parameter λ is

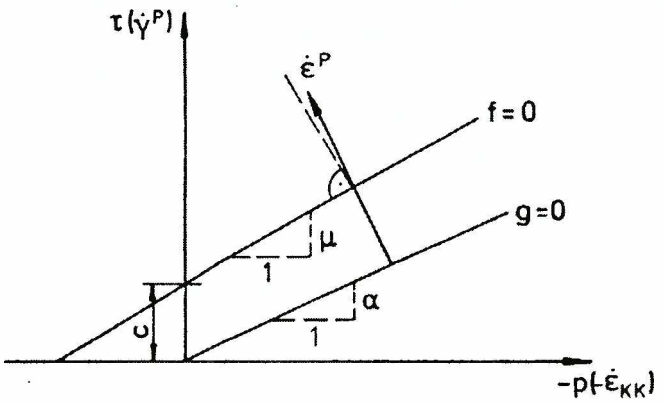

Figure 4.1. *Yield and flow potential curves in the τ, p-plane*

calculated from the consistency condition $df = 0$. The expression for τ in Eq. 4.5 can be determined with the aid of the plastic shear strain rate $\dot{\gamma}^p$ which has been derived on the macroscopic level by taking into account slip and rotation in a random assembly of circular rods with a diameter d_{50} (Mühlhaus 1987):

$$\dot{\gamma}^p = (3\dot{e}_{ij}^p \dot{e}_{ij}^p - \dot{e}_{ij}^p \dot{e}_{ji}^p + d_{50}^2 \dot{\kappa}_i^p \dot{\kappa}_i^p)^{0.5}, \tag{4.8}$$

where $\dot{e}_{ij}$ is the deviatoric part of the non-symmetric deformation rate tensor $\dot{\varepsilon}_{ij}$. Assuming that τ and $\dot{\gamma}^p$ are work-conjugate (Mühlhaus 1987)

$$\tau \dot{\gamma}^p = s_{ij} \dot{e}_{ij} + m_i \dot{\kappa}_i, \tag{4.9}$$

τ in Eq.4.5 and the coefficients $a_1 = 3/8$, $a_2 = 1/8$ and $a_3 = 1$ can be found. If the moment stress vector m_i vanishes, τ in Eq. 4.5 is reduced to its counterpart in a non-polar continuum,

$$\tau = (s_{ij} s_{ij})^{0.5}. \tag{4.10}$$

Other combinations of the constants a_1, a_2 and a_3 are also theoretically possible, provided that $a_1 + a_2 = 0.5$ (Mühlhaus 1990). The constants $a_1 = 3/8$, $a_2 = 1/8$ and $a_3 = 1$ turned out as useful and sufficient in numerical calculations involving

localisation (Tejchman 1989). In general, the constants a_1, a_2 and a_3 control the influence of Cosserat quantities on the material behaviour. The larger the difference between a_1 and a_2, the larger the non-symmetry of the stress tensor and the larger the effect of Cosserat quantities on the material behaviour (Tejchman and Wu 1993). The influence of a_3 on the results is rather insignificant.

The factors μ in Eq. 4.6 and α in Eq. 4.7, which are related to the angle of internal friction Φ and the angle of dilatancy β of granular materials, can be identified with the help of tests in a plane strain apparatus (Vardoulakis 1980). Figure 4.2 shows the general mobilised friction factor μ and the mobilised dilatancy factor α for dense granular materials. The function describing the mobilised friction factor μ versus the plastic shear deformation γ^p was proposed by Vardoulakis (1980) on the basis of the biaxial tests:

$$\mu = \mu_{cr} - (\mu_{cr} - c_1\gamma^p)\exp(-c_2\gamma^p), \tag{4.11}$$

wherein $\mu_{cr} = \sin\Phi_{cr}$ is the friction factor in a residual state, Φ_{cr} denotes the critical angle of internal friction, and c_1 and c_2 are the constants which are calculated from two simple conditions fulfilled at the peak of the curve:

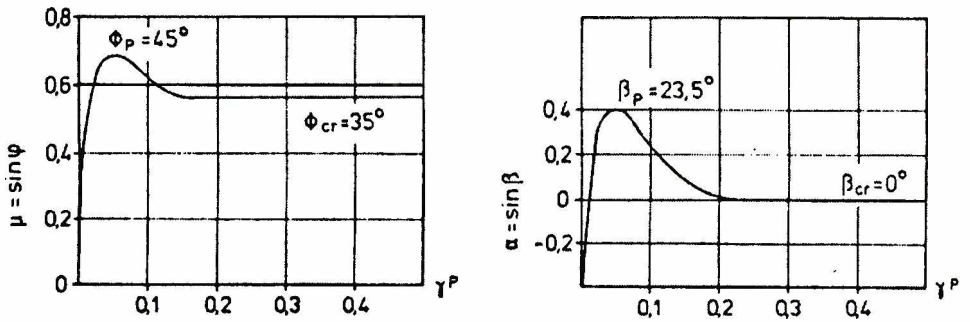

Figure 4.2. *Mobilised friction factor μ and mobilised dilatancy factor α for dense granular material (Φ — angle of internal friction, β — dilatancy angle, γ^p — plastic shear deformation, subscript «p» — peak value, subscript «cr» — critical value)*

$$\mu(\gamma_p^p) = \sin\phi^p, \qquad \frac{\partial\mu}{\partial\gamma^p}(\gamma_p^p) = 0. \tag{4.12}$$

Φ^p and γ_p^p denote the maximum angle of internal friction and the corresponding plastic shear deformation, respectively. For the function α versus γ^p, the following relation was assumed (Tejchman 1989):

$$\alpha = 3(\mu - \mu_{cr}). \tag{4.13}$$

The outlined constitutive law includes 7 material constants which are to be determined, viz.: E, ν, Φ^p, Φ_{cr}, γ_p^p and d_{50}.

The capability of an elasto-plastic Cosserat model in solving various boundary value problems involving localisation was demonstrated by Tejchman (1989, 1994,

1997, 1998), Mühlhaus (1989, 1990), de Borst (1991), Papanastasiou and Vardoulakis (1992), Sluys (1992), Tejchman and Wu (1993, 1995, 1997), Tejchman and Gudehus (1993), Unterreiner et al. 1994, Steinmann (1995), Murakami and Yoshida (1997) and Groen (1997).

5. Polar Boundary Conditions on the Wall

The Cosserat boundary conditions in a polar continuum allow for the different wall roughness with consideration of Cosserat rotations. According to Yoshimi and Kishida (1981), and Uesugi (1987), the roughness of the wall can quantitatively be characterised by the average distance from the peak to the valley of asperities, r_w, measured on a representative surface of 2.5 cm × 2.5 cm. However, it is the roughness ratio between the wall roughness and the mean grain diameter, r_w/d_{50}, that determines the interface behaviour between the wall and the granulate (Tejchman 1989). The walls are smooth if the roughness r_w is almost equal to zero ($r_w/d_{50} \approx 0$), rough if the roughness is larger than zero but smaller than d_{50}, i.e. $r_w/d_{50} < 1$) and very rough if the roughness is larger or equal to d_{50}, i.e. $r_w/d_{50} \geq 1$). For modelling of very rough walls in silos, full shearing of the material along a rigid wall is assumed:

$$u_1 = 0\,,\; u_2 = 0\,,\; \omega^c = 0. \tag{5.1}$$

The assumption $u_2 = 0$ was confirmed by model tests (Tejchman 1989). A slip along very rough walls occurred only if the wall friction angle reached its residual value and at the same time no deformations in the material were observed. Up to this point, the material experienced shearing. The condition ω^c was verified during shearing tests in a Couette apparatus with steel rods representing sand grains (Tejchman 1989). In the case of rough and smooth silo walls, both shearing and slip of the material along a rigid wall are taken into account. The calculations are carried out with the following assumptions (Fig.5.1):

$$u_1 = 0\,,\; \omega^c / u_2 = r_w / d_{50}^2\,. \tag{5.2}$$

The third condition assuming a relation between the curvature and the displacement gradient is obtained automatically. The ratio r_w/d_{50} is assumed to be 0.0001 for smooth walls and 0.1–0.5 for rough walls. The assumed boundary conditions in Eq. 5.2 are realistic and consistent, i.e. for $r_w/d_{50} \approx 0$, no stress changes in the material are observed, and for $r_w/d_{50} = 1$, the numerical results approach the results for very rough walls with the boundary conditions expressed by Eq. 5.1. As a result of the polar boundary conditions on the wall, the wall friction angle is derived and no special interface elements are needed (Tejchman 1997).

5. Finite Element Implementation

For the numerical simulations, the following material constants for glass beads were used: $\rho = 1700$ kg/m^3, $\nu = 0.3$, $\Phi^p = 30^\circ$, $\Phi_{cr} = 29^\circ$, $\beta^p = 2.5^\circ$ and $d_{50} = 2.3$ mm. The values of ν, Φ^p and Φ_{cr} were determined with compression tests performed by

Wu (1992) for similar glass beads. The modulus of elasticity, $E = 1000$ kPa, was adapted on the basis of the test data in a hopper (Section 2) to approximately obtain a similar frequency of longitudinal stress waves which are dominant in silos with smooth walls (Tejchman 1989). In general, E is estimated on the basis of resonant column tests (Das 1983).

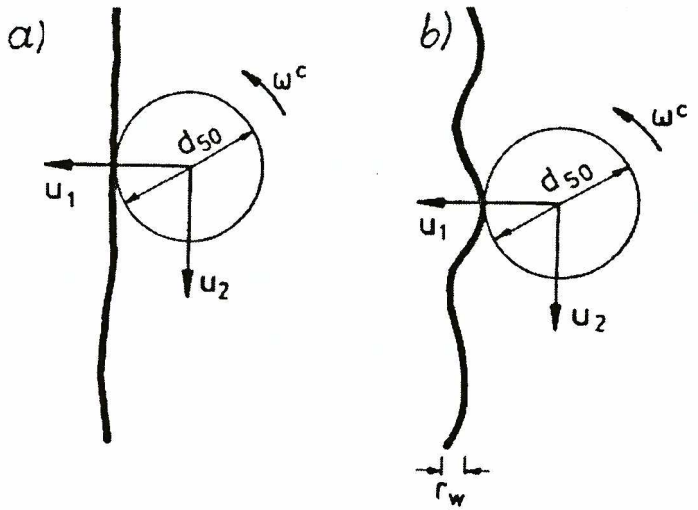

Figure 5.1. *Kinematics along a smooth (a) and a rough silo wall (b)*

For the plane strain calculations, 400 quadrilateral finite elements composed of four diagonally crossed triangles were applied to avoid volumetric locking and spurious element behaviour (Groen 1997). Totally, 1600 triangular elements with linear shape functions for the displacements and the Cosserat rotation were used. Symmetry with respect to the centreline was taken into account. The width of FE-elements along the wall was equal to d_{50}.

The calculations were performed with a lumped mass matrix (Bathe 1982). The volume body moment m^B (Eq. 3.20) was neglected. The initial calculations showed that $m^B = \pm\gamma_d(d_{50}/2)$ had an insignificant influence on the results. The volume inertia moment $\theta = 0.5\rho\,(d_{50}/2)^2$ was assumed as for a cylinder with a diameter d_{50}.

To capture the possibility of energy loss during the inelasticity of grain collisions, linear viscous damping matrix C was included. It was constructed using the global mass matrix M, $C = 2\eta M$, where η [s^{-1}] is the linear damping coefficient.

To model free silo outflow due to gravitation, the supporting forces along the outlet due to the filling process were reduced to zero from the beginning of the flow. As the initial stress state, the K_o-state was assumed ($\sigma_{22} = \gamma_d x_2$, $\sigma_{11} = K_o\sigma_{22}$, $\sigma_{12} = \sigma_{21} = 0$, $\gamma_d = \rho g = 16.68$ kN/m^3, $K_o = 0.4$), x_2 is the vertical coordinate measured from the top of the silo fill and γ_d denotes the material density. The boundary conditions of the silo fill were along the top traction and moment free.

They were in the symmetry axis: $u_1 = 0$, $\omega_c = 0$, $\sigma_{21} = 0$. The wall was assumed to be very smooth (as in the experiment), $r_w/d_{50} = 0.0001$.

The calculations were carried out mainly with small deformations and curvatures. However, some analyses were performed for large deformations and curvatures by an Updated Lagrangian formulation (Bathe 1982) using both the Jaumann stress rate and Jaumann couple stress rate. At the same time, the changes of the element configuration and the element volume were taken into account.

To satisfy the consistency condition $f = 0$, the trial stress method (linearised expansion of the yield condition about the trial stress point) using an elastic predictor and a plastic corrector with radial return mapping algorithm (Ortiz and Simo 1986) was applied.

For the solution of the non-linear equation of motion governing the response of a system of finite elements, an implicit integration method by Newmark with a modified Newton-Raphson scheme was used (Bathe 1982). The calculations were performed using a symmetric elastic global stiffness matrix. The iteration steps were performed using translation and rotation convergence criteria (found by means of preliminary FE-calculations) and a criterion on the minimum number of iterations (at least 12) in each time step. The time increment was chosen as 0.0005 s.

The tensile normal stresses were not allowed in the silo fill. If they were obtained in elements above the outlet, the normal stresses, shear stresses and couple stresses in these elements were replaced by values equal to zero. For such elements, the element stiffness matrix was assumed to be equal to the initial elastic one.

7. Numerical Results

Figs.7.1–7.7 show some numerical results for a model hopper with smooth walls under conditions of both small and large deformations and curvatures. The viscous damping was not taken into account.

The numerical results (Figs.7.1 and 7.2) show that the calculated pulsations in the glass beads are almost harmonic and are close to those from the experiments. The pulsations are connected to natural vibrations of a silo fill induced by disturbances of flow at the outlet (Hatamura and Takeuchi 1989, Tejchman 1997, 1998). The pulsations are created at the bottom and propagate upwards in the form of stress waves. In silos with smooth walls, longitudinal waves are dominant. The stress waves are created due to the change of the direction of shear deformation at the outlet that is connected to alternate volume changes (Tejchman 1997). The volume changes are connected to the stress changes that lead to the formation of dynamic pulsations due to the presence of inertial forces. The amplitude from peak to peak of the calculated wall normal stress at the mid-point on the wall is about 0.8 kPa, and is in a satisfactory agreement with the experimental value of 0.6 kPa. However, the calculated mean wall normal stress, 0.8 kPa, is twice as high as the experimental result. The amplitude from peak to peak of the calculated vertical normal stress inside the material is about 2.0 kPa The pulsations of the wall shear

stress are almost insignificant. The calculated frequency of pulsating stresses, $f = 14$ Hz, is too high. To better approximate the frequency of dynamic effects and the mean wall stress, the modulus of elasticity should be slightly reduced, and the calculations should be performed with consideration of the filling process which induces wall shear stresses. The calculated frequency can be obtained with the formula for the fundamental frequency of the longitudinal vibration in an elastic bar of a silo height with the top and bottom free using the wave equation (Das 1983).

$$f = \sqrt{\frac{E(1-\nu)}{\rho(1+\nu)(1-2\nu)}}/2h = \sqrt{\frac{1000\ (1-0.3)}{1.7(1+0.3)(1-2\cdot 0.3)}}/2\cdot 0.9 \cong 14\text{Hz} \qquad (7.1)$$

The calculated vertical displacements u_2 and velocities $\dot{u}_2$ are very similar in the entire flowing material due to small friction along the walls. They strongly increase with flow time (Fig.7.1). At $t = 0.5$ m/s, $u_2 = 0.6$ m and $u_2 = 2.4$ m/s. The calculated

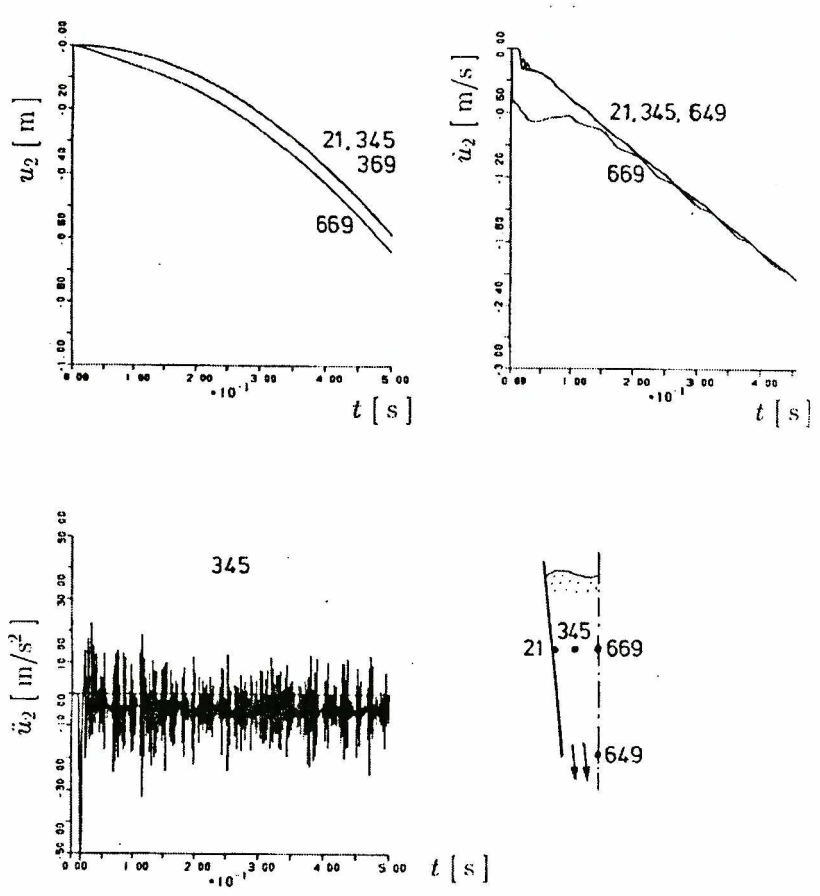

Figure 7.1. *Calculated vertical displacement u_2, vertical velocity $\dot{u}_2$ and vertical acceleration $\ddot{u}_2$ in glass beads during flow*

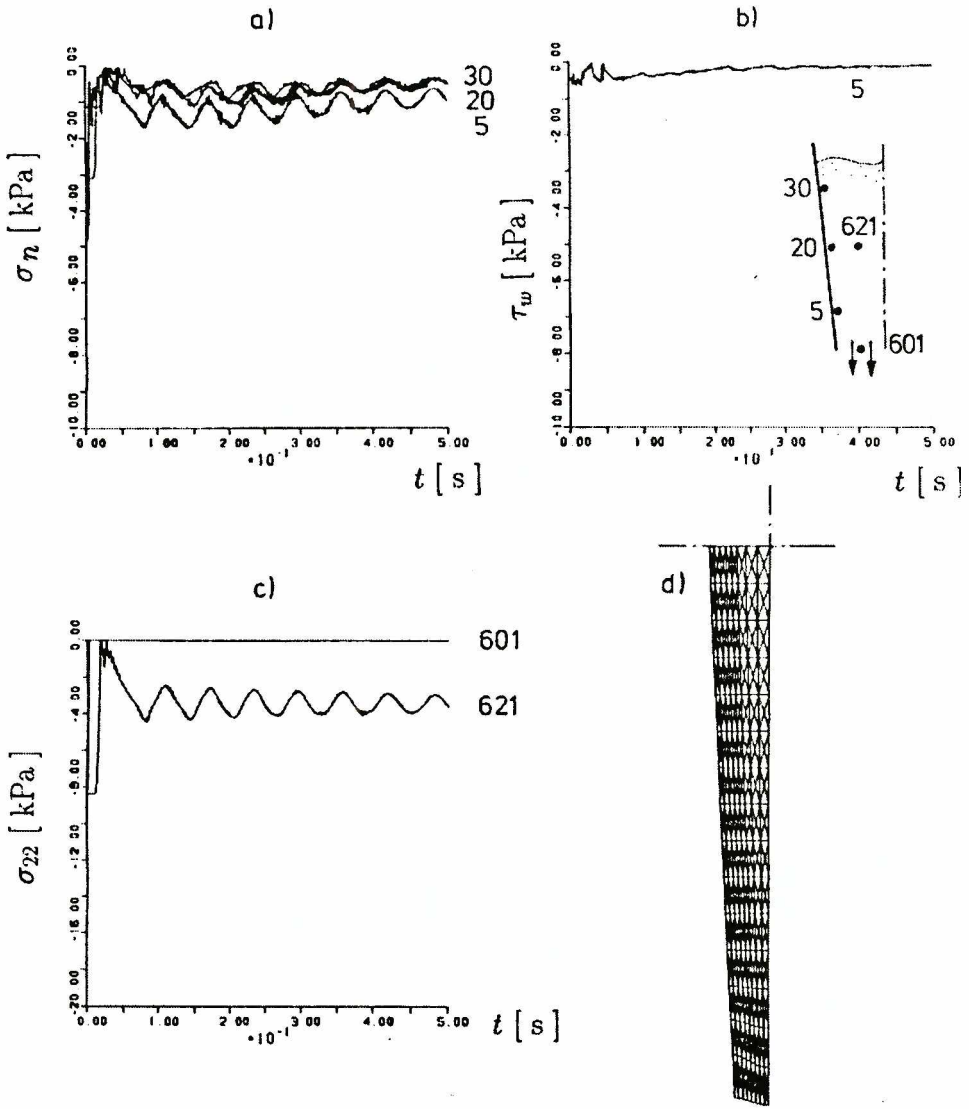

Figure 7.2. *Calculated normal stress σ_n on the wall (a), wall shear stress τ_w, vertical normal stress σ_{22} inside the fill (c) during flow of glass beads and deformed mesh (d) in the lower part of the hopper at t = 0.5 s*

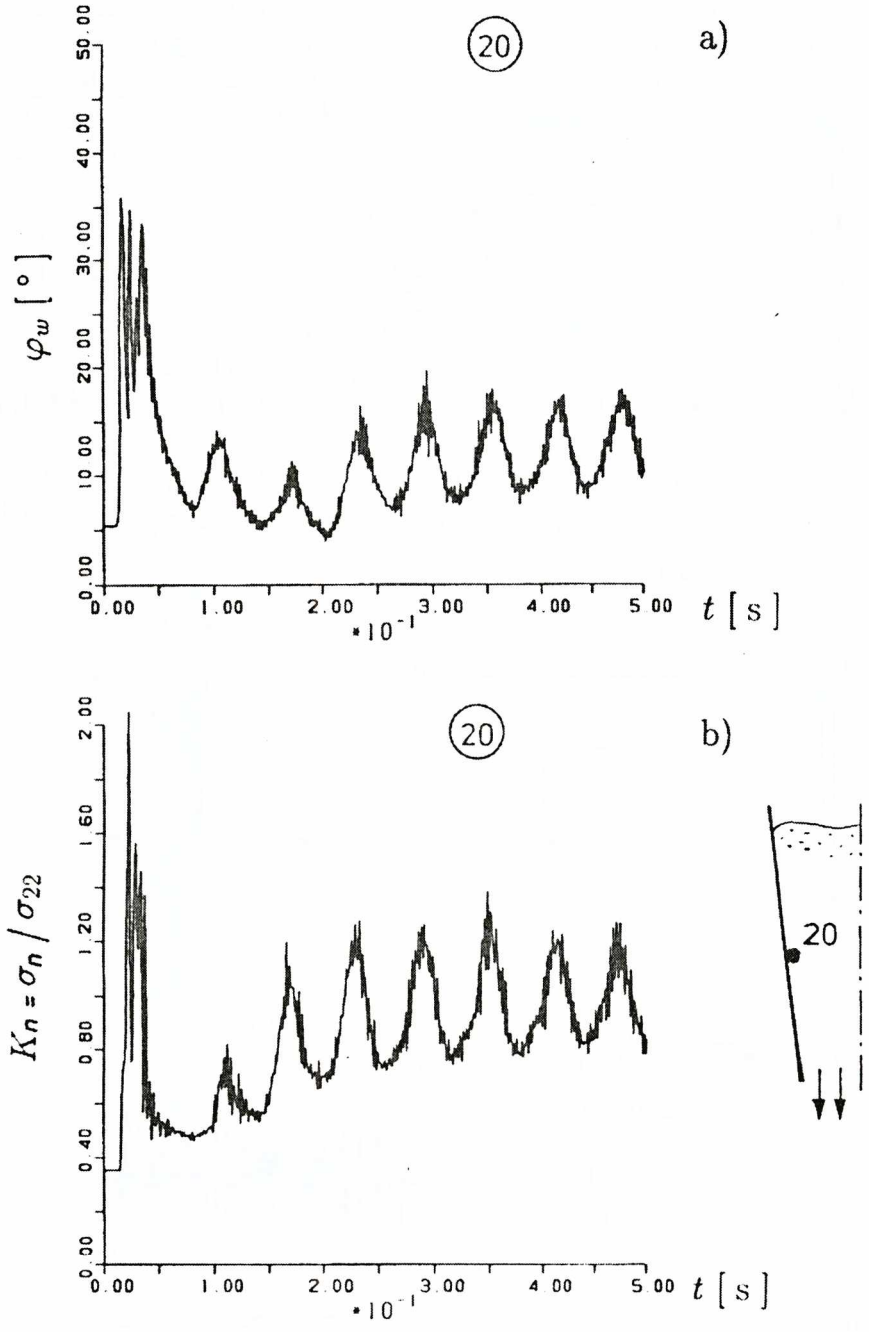

Figure 7.3. *Calculated wall friction angle $\varphi_w = \arctan(\tau_w/\sigma_n)$ (a) and wall pressure coefficient $K_n = \sigma_n/\sigma_{22}$ (b) during flow of glass beads*

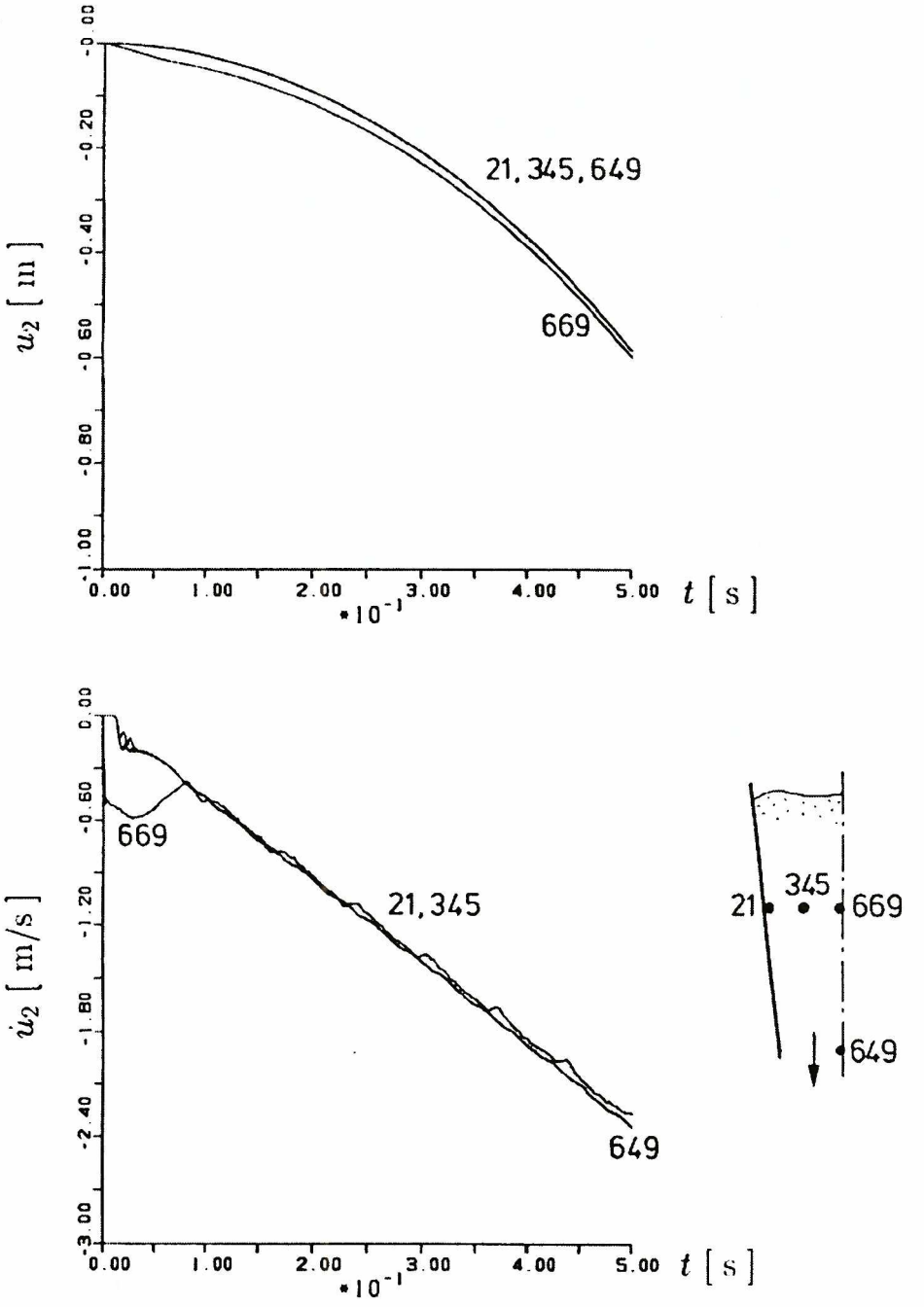

Figure 7.4. *Calculated vertical displacement u_2 and vertical velocity $\dot{u}_2$ in glass beads during flow (large deformations and curvatures)*

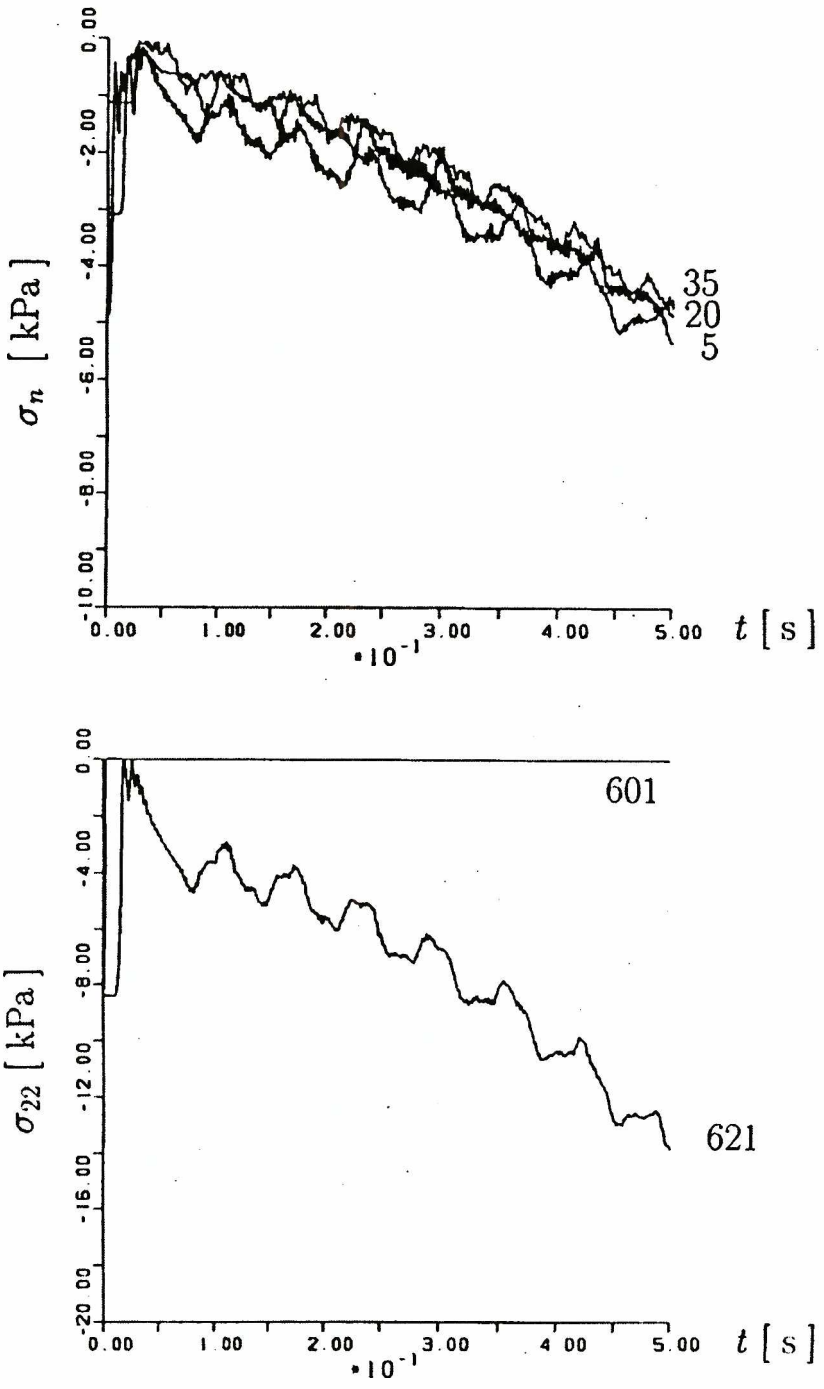

Figure 7.5. *Calculated normal stress σ_n on the wall and vertical normal stress σ_{22} inside the fill during flow (large deformations and curvatures)*

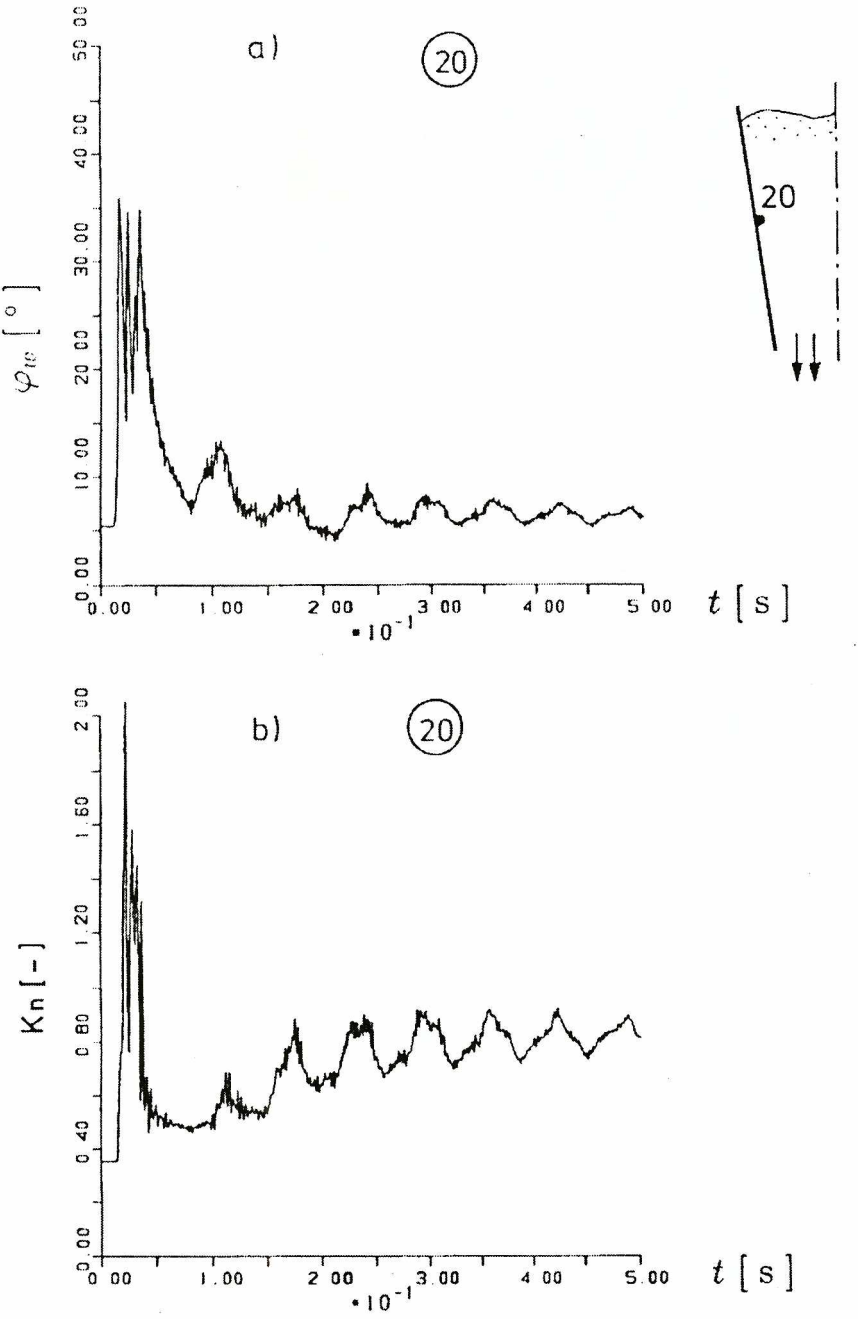

Figure 7.6. *Calculated wall friction angle $\varphi_w = \arctan(\tau_w/\sigma_n)$ (a) and wall pressure coefficient $K_n = \sigma_n / \sigma_{22}$ (b) during flow (large deformations and curvatures)*

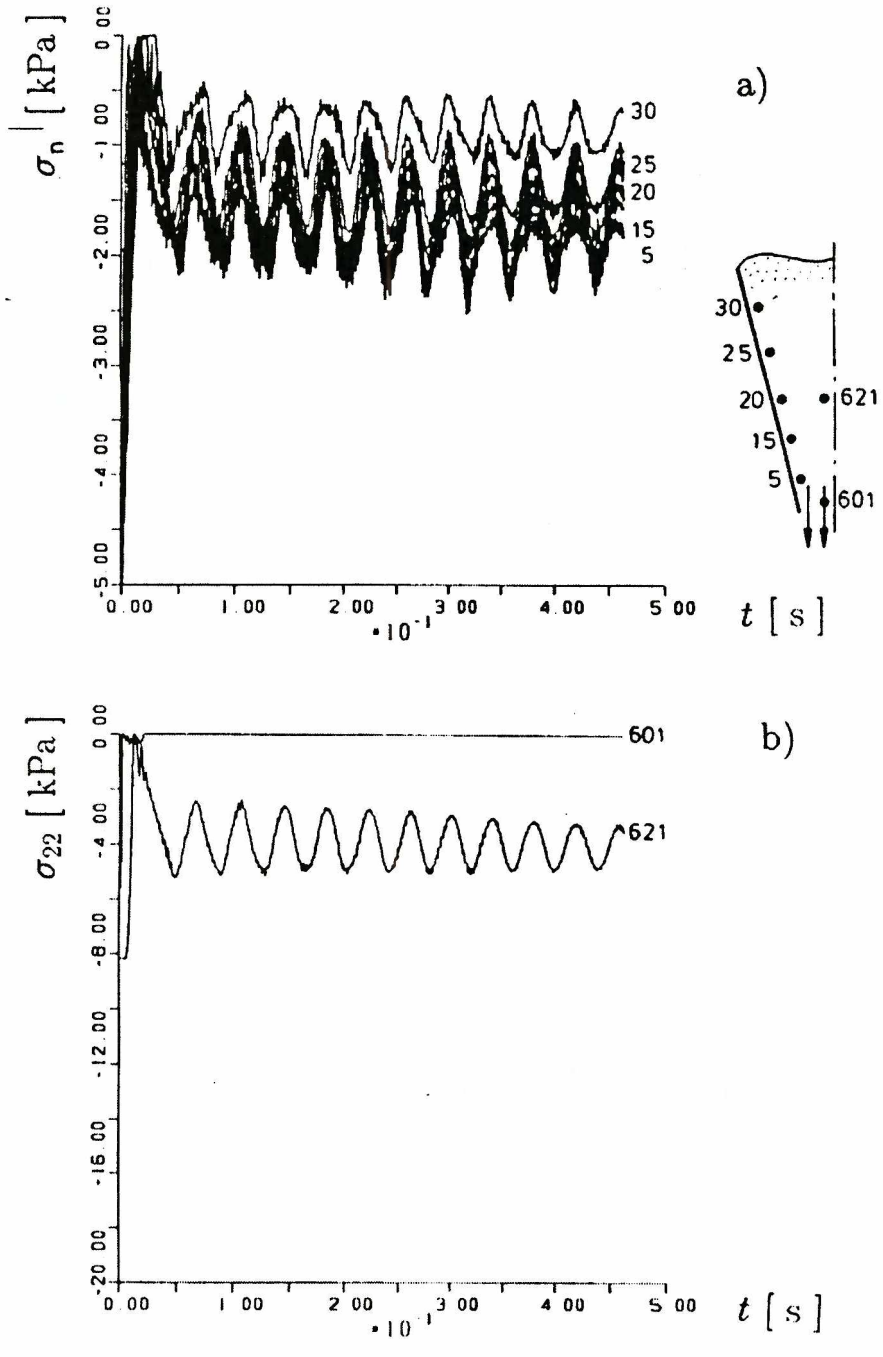

Figure 7.7. *Calculated normal stress σ_n on the wall and vertical normal stress σ_{22} inside the fill during flow of glass beads (E = 2000 kPa)*

velocities differ markedly from the experimental value of $v = 0.3$ m/s. The calculated vertical acceleration inside the material oscillates around the gravitational acceleration g (Fig.7.1). The value of the vertical acceleration from peak to peak is about 3g.

The material moves almost as a rigid body due to small wall friction. The thickness of the wall shear zone is approximately equal to d_{50} (Fig.7.2).

For a better agreement of the calculated mean wall friction angle, $\varphi_w = 12^\circ$ (Fig.7.3), with the measured result of $\varphi_w = 18.4^\circ$ at the mid-point of the wall, the coefficient r_w/d_{50} should be slightly increased in the wall boundary condition. The calculated mean pressure coefficient $K_n = \sigma_n/\sigma_{22}$ is about 0.9 (Fig.7.3).

The consideration of large deformations and curvatures does not influence the results of the displacements, velocities (Fig.7.4), mean wall friction angle and mean pressure coefficient (Fig.7.6). That has, however, a large effect on the mean horizontal normal stress on the wall (Fig.7.5) which increases continuously during flow (due to updating of the body volume). One has to remember that the material height in model tests was decreasing during flow whereas it remained constant in the FE-calculations.

An increase of E by the factor 2 increases the amplitude of normal stresses on the wall by 10% and the frequency of pulsations to $f = 24$ Hz (Fig.7.7).

The numerical results with consideration of a linear viscous damping in the silo fill ($\eta = 10$ s^{-1}) are shown in Fig.7.8. At $t = 0.5$ s, $u_2 = 0.2$ m and $\dot{u}_2 = 0.4$ m/s. After $t = 0.1$ s, the vertical velocity $\dot{u}_2$ in the glass beads reaches almost a constant value (its increase is insignificant). The obtained result of $\dot{u}_2$ is, thus, in accordance with the experiment. The consideration of a linear viscous damping during flow causes also a decrease of amplitudes of pulsating wall stresses. At the same time, the mean stresses do not change.

The effect of d_{50} in the range of 2.3–4 mm was found to be insignificant on the FE-results.

8. Discussion

The numerical results show that the onset of rapid silo flow can be realistically described with a polar elasto-plastic constitutive law on condition that the elastic modulus and the viscous damping coefficient are known. Their effect on the flow velocity and stress amplitudes is of importance. However, there is not enough experimental data on these two parameters.

Rapid gravitational flow is not easy for numerical modelling for the longer flow time with the used continuum model due to an increasing distortion of the FE-mesh and increasing tensile regions inside the flowing material above the outlet. Therefore only the onset of rapid flow can be simulated. The problem of a large distortion of the FE-mesh can be dealt with twofold. A mixed Euler-Lagrangian procedure opens one way. In contrast with an Updated Lagrangian formulation, it allows for the mesh distortion since the material displacements are uncoupled from the nodal point

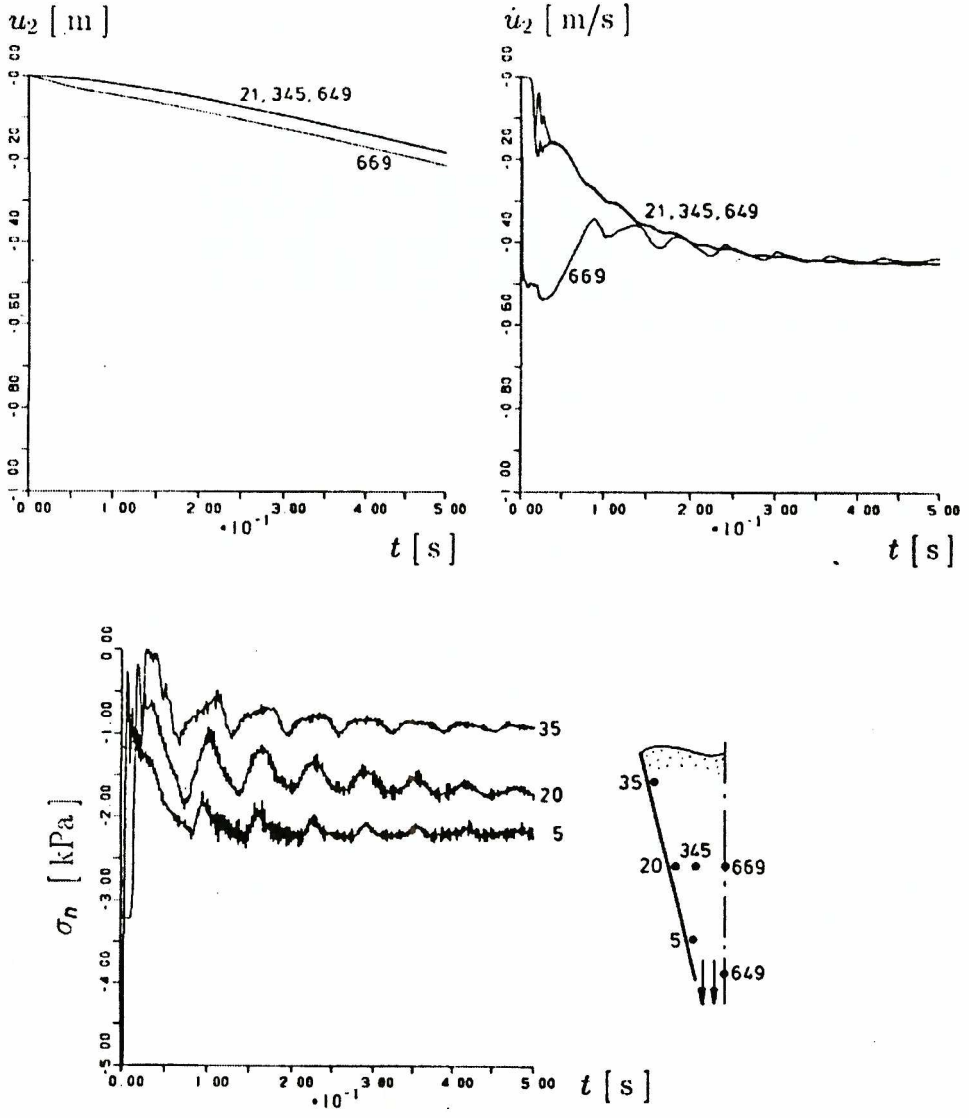

Figure 7.8. Calculated vertical displacement u_2, vertical velocity $\dot{u}_2$ and normal stress on the wall σ_n in glass beads during flow (η =10 s^{-1})

displacements (Hueting and Helm 1992, van den Berg 1994). The material streams through the mesh and the geometry of finite elements is fixed. This method can be used by an extension of a conventional Lagrangian formulation by adding convective terms proportional to the relative displacement increments. Another possibility is the application of the so-called "dead elements" option. The elements which have already passed through the silo outlet are cut off. The avoidance of the tensile regions is not possible since the constitutive law is designated for deformation rates

at which grain do not lose contacts. The assumption of too large damping can suppress dynamic pulsations in a silo (Tejchman 1997) Thus, there is a need for a new constitutive law capable to capture the material behaviour in the regime of slow and rapid flow. As outlined by Mühlhaus et al. (1995), an extension of a FEM based on a constitutive continuum model for slow flow by terms of a kinetic theory by Haff (1993) is feasible.

References

[1] Airy W., *The pressure of grain*, Proc. Inst. of Civil Engineering, London, 131, 347-358, 1897

[2] Bathe K. J., *Finite Element Procedures in Engineering Analysis*, Prentice-Hall, Inc., Englewood Cliffs, New Jersey, 1982

[3] Baxter G. W., Behringer R. P., *Pattern formation and time-dependence in flowing sand*, Two Phase Flows and Waves, Springer Verlag, New York, 1-29, 1990

[4] Becker M., Lippmann H., *Plane plastic flow of granular model material, experimental set-up and results*, Archives of Mechanics, Warszawa, 29, 829-846, 1977

[5] Benallal A., Billardon R., Geymonat G., *Localization phenomena at the boundaries and interfaces of solids*, Proc. 3rd Int. Conf. Constitutive Laws for Engineering Materials: Theory and Applications,Tucson, Arizona, 387-390, 1991

[6] van den Berg P., *Analysis of soil penetration*, Dissertation, Delft University, 1-175, 1994

[7] Bogdanova-Bontscheva N., Lippmann H., *Rotationssymmetrisches ebenes Fliessen eines granularen Modellmaterials*, Acta Mech., 21, 93-113, 1975

[8] de Borst R., *Simulation of localisation using Cosserat theory: a reappraisal of the Cosserat continuum*, Engng. Comput. 8, 317-332, 1991

[9] de Borst R., Mühlhaus H. B., Pamin J., Sluys L. Y., *Computational modelling of localization of deformation*, Proc. 3rd Int. Conf. Comp. Plasticity, eds.: D. R. J. Owen, E. Onate and E. Hinton, Pineridge Press, Swansea, 483-508, 1992

[10] Buggisch H., Renner M., *Theoretische und experimentele Untersuchungen zum schnellen Fließen von Schüttgütern in konvergenten Geometrien*, SFB „Silos", Karlsuhe University, 65-86, 1993

[11] Cundall P. A., Strack O. D. L., *A discrete numerical model for granular assemblies*, Geotechnique, 29, 47-65, 1979

[12] Das M. B., *Fundamentals of Soil Dynamics*, New York, Elsevier, 1983.

[13] Drescher A., *Metody obliczeń parć i przepływu materiałów ziarnistych w zbiornikach*, Polska Akademia Nauk, Warszawa-Poznan, 1983

[14] Eibl J., Rombach G., *Consistent Modelling of Filling and Discharging Processes in Silos*, Intern. Conf. Silos-Forschung und Praxis, Universität Karlsruhe, SFB 219, 1-15, 1988

[15] Enstad G., *On the Theory of Arching in Mass Flow Hoppers*, Chem. Engng. Sci. 30, 1975

[16] Fröhlich O. K., *Die Druckverteilung in der Silozelle und im Baugrunde*, Beton und Eisen, Berlin, 1934

[17] Fütterer G., *Untersuchungen zum schnellen Fließen von trockenen, kohäsionslosen Schüttgütern in konvergenten Schächten*, Dissertation, Karlsruhe University, 1-140, 1991

[18] Groen A. E., *Three-dimensional elasto-plastic analysis of soils*, Dissertation, Delft University, 1-113, 1997

[19] Gudehus G., Tejchman J., *Some mechanisms of a granular mass in a silo - model tests and a numerical Cosserat approach*, Advances in Continuum Mechanics, eds.: O. Brüller, V. Mannel, J. Najar (dedicated to H. Lippmann), Springer Verlag, Berlin, Heidelberg, 178-193, 1991

[20] Gutfraind R., Pouliquen O., *Study of the origin of shear zones in quasi-static vertical chute flows by using discrete particle simulations*, Mechanics of Materials, 24, 273–285, 1996

[21] Günther W., *Zur Statik und Kinematik des Cosserat-Kontinuums*, Abh. Braunschweigische Wiss., 10, 1958

[22] Haff P. K., *Grain flow as a fluid - mechanical phenomenon*, J. Fluid Mech. 134, 401–430, 1983

[23] Hatamura Y., Takeuchi T., *Analysis of physical phenomena in silos, Powders and Grains*, eds.: J. Biarez, R. Gourves, Balkema, Rotterdam, 445-452, 1989

[24] Häußler U., Eibl J., *Numerical investigation of discharging silos*, J. Engineering Mechanics, 110, 975-971, 1984

[25] Horn R. M., Nedderman R. M., *Analysis of the stress distribution in two-dimensional bins by the method of characteristic*, Powder Technology, 14, 1976

[26] Huetink J., van der Helm P., *On Euler-Lagrange finite element formulation in forming and fluid problems*, Proc. NUMIFORM, eds.: Chenot et al., Balkema, Rotterdam, 45-54, 1992

[27] Jenike A. W., *Storage and Flow of Solids*, Utah Eng. Exp. Stat. Bull. 123, 1964

[28] Jenkins J. T., Richman M. W., *Kinetic theory for plane flows of a dense gas of identical, rough, inelastic, circular disks*, Phys. Fluids, 28, 3485-3494, 1985

[29] Jenkins J. T. *Boundary conditions for rapid granular flow: flat, frictional walls*, Journal of Applied Mechanics, 59, 120-127, 1992

[30] Kafui K. D., Thornton C., *Some aspects of silo discharge: computer simulations*, PARTEC95, Nürnberg, 379-388, 1995

[31] Kafui K. D., Thornton C., *Some observations on granular flow in hoppers and silos*, Powders and Grains, eds.: Behringer, Jenkins, Balkema, Rotterdam, 511-514, 1997

[32] Kanatani K., *A micropolar continuum theory for granular materials*, Int. J. Eng. Sci., 17, 419-432, 1979

[33] Langston P. A., Heyes D. M., Tüzün U., *Discrete Element Simulation of Granular Flow in Hoppers*, Proc. of the 3rd European Symposium Storage and Flow of Particulate Solids, PARTEC 95, Nürnberg, Germany, 357-367, 1995

[34] Löffelmann F., *Theoretische und experimentelle Untersuchungen zur Schüttgut-Wand-Wechselwirkung und zum Mischen und Entmischen von Granulaten*, Dissertation, Universität Karlsruhe, 1989

[35] Lin X., Nakagawa M., Mustoe G., *Simulations on hopper flows of elongated particles*, Proc. 5th World Congress of Chemical Engineering, San Diego, 5, 367-373, 1996

[36] Luding S., Duran J., Clement E., Rejchenbach J., *Computer simulations and experiments of dry granular media: polydisperse disks in a vertical pipe*, Proc. 5th World Congress of Chemical Engineering, San Diego, 5, 325-330, 1996

[37] Lun C. K. K., Savage S. B., *A simple kinetic theory for granular flow of rough, inelastic spherical particle*, J. Appl. Mech. 54, 47-53, 1987

[38] Masson S., Martinez J., Deserable D., *Comparative simulations of particle flow using a distinct element method and a lattice grain model*, Proc. 5th World Congress of Chemical Engineering, San Diego, 5, 349-355, 1996

[39] Martinez J., Masson S., Deserable D., *Flow Patterns and Velocity Profiles during Silo Discharge Simulation with a Lattice Grain Model*, Proc. of the 3rd European Symposium Storage and Flow of Particulate Solids, PARTEC 95, N(rnberg, Germany, 367-379, 1995

[40] Melix P., *Stabilitätsprobleme bei der Siloentleerung*, Int. Report SFB 219, University Karlsruhe, 1985

[41] Mindlin R. D., *Microstructure in linear elasticity*, Arch. Rat. Mech. Anal., 16, 51-78, 1964

[42] Mróz Z., *Non-associated Flow Laws in Plasticity*, J. de Mechanique, 1, 21-42, 1963

[43] Mróz Z., Szymański C., *Gravity flow of a granular material in a converging channel*, Archives of Mechanics, 23, 6897-917, 1971

[44] Murakami A., Yoshida N., *Cosserat continuum and finite element analysis*, Deformation and Progressive Failure in Geomechanics, eds.: A. Asaoka, T. Adachi anf F. Oka, Pergamon, 871-876, 1997.

[45] Mühlhaus H. B., *Berücksichtigung von Inhomogenitäten im Gebirge im Rahme einer Kontinuumstheorie*, Veröffentlichungen des Institutes für Boden- und Felsmechanik, Universität Karlsruhe, 106, 1987

[46] Mühlhaus H. B., Vardoulakis, I., *The thickness of shear bands in granular materials*, Geotechnique, 37, 271-283, 1987

[47] M(hlhaus H. B., *Stress und couple stress in a layered half plane with surface loading*, Int. Jour. for Numer. and Analyt. Met. in Geomech., 13, 545-563, 1989

[48] Mühlhaus H. B., *Application of Cosserat theory in numerical solutions of limit load problems*, Ing. Arch., 59, 124-137, 1989

[49] Mühlhaus H. B., *Continuum models for layered and blocky rock, Comprehensive Rock Engineering*, eds.: J. A. Hudson, Ch. Fairhurst, Pergamon Press, 2, 209-231, 1990

[50] Mühlhaus H. B., Chin Hsin Li, Hornby P., *Solid-Fluid Transition in Granular Flow: Constitutive and Computational Aspects*, Felsmechanik Kolloquium, University Karlsruhe, 1995

[51] Oda M., Konishi, Nemat-Nasser S., *Experimental micromechanical evaluation of strength of granular materials*, effects of particle rolling, Mechanics of Materials, North-Holland Publishing Comp., 1, 269-283, 1982

[52] Oda M., *Micro-fabric and couple stress in shear bands of granular materials*, Powders and Grains, ed.: C. Thornton, Rotterdam, Balkema, 161-167, 1993

[53] Ortiz M., Simo I. C., *An analysis of a new class of integration algorithms for elastoplastic constitutive relation*, Int. J. Numer. Methods in Engrg. 23, 353-366, 1986

[54] Papanastasiou P., Vardoulakis I., *Numerical treatment of progressive localization in relation to borehole stability*, Int. J. Num. Anal. Meth. Geomech., 16, 389-424, 1992

[55] Pouliquen O., Gutfraind R., *Stress fluctuations and shear zones in quasistaic granular chute flows*, Physical Review, 53, 552-561, 1996

[56] Ragneau E., Aribert J. M., *General recurrent determination of grain action along silo walls during filling, transient flow and permanent emptying*, Proc. of the 3rd European Symposium on Storage and Flow of Particulate Solids, PARTEC95, Nürnberg, 205-219, 1995

[57] Renner M., *Über die Stabilität der stationären Strömung von Schüttgütern in vertikalen Schächten*, Dissertation, Faculty of Chemistry, Karlsruhe University, 1-166,1996

[58] Ristow G. H., *Outflow rates and stresses in 3D hoppers*, eds.: Behringer and Jenkins, Balkema, Rotterdam, 527-530, 1997

[59] Ruckenbrod C., Eibl J., *Dynamic Phenomena in Discharging Silos*, Proc. of the 3rd European Symposium Storage and Flow of Particulate Solids, PARTEC 95, Nürnberg, Germany, 193-202, 1995

[60] Sakaguchi H., Ozaki E., *Analysis of the formation of arches plugging the flow of granular materials*, Powders and Grains, eds.: C. Thornton, Balkema, Rotterdam, 351-357, 1993

[61] Savage S. B., Jeffrey D. J., T*he stress tensor in a granular flow at high shear rates*, J. Fluid Mech., 110, 255-272, 1981

[62] Savage S. B., *Numerical Simulations of Couette Flow of Granular Materials: Spatio-Temporal Coherence of 1/f Noise*, Physics of Granular Media, eds.: D. Bideau, J. Dodds, Nova Science Publishers Inc. 343-362, 1992

[63] Schäfer H., *Versuch einer Elastizitätstheorie des zweidimensionalen ebenen Cosserat-Kontinuums*, Miszellaneen der Angewandten Mechanik, Festschrift Tolmien, W., Berlin, Akademie-Verlag, 1962.

[64] Schwedes J., *Fließverhalten von Schüttgütern in Bunkern*, Weinheim, 1968

[65] Sluys L. J., *Wave propagation, localisation and dispersion in softening*, Dissertation, Delft University, 1-163, 1992

[66] Steinmann P., *Theory and numerics of ductile micropolar elastoplastic damage*, Int. Journal for Numerical Methods in Engineering, 38, 583-606, 1995

[67] Tano E., Godoy L. A, Diez M. A., *Numerical modelling of the flow of solids stored in silos, Computer Methods and Advances in Geomechanics*, eds.: H. J. Siriwardane, M. M. Zaman, 2, 1281-1291, 1994

[68] Tejchman K., *Scherzonenbildung und Verspannungseffekte in Granulaten unter Berücksichtigung von Korndrehungen*, Veröffentlichungen des Institutes für Boden- und Felsmechanik, Universität Karlsruhe, 117, 1-236, 1989

[69] Tejchman J., Wu W., *Numerical study on shear band patterning in a Cosserat continuum*, Acta Mech., 99, 61-74, 1993

[70] Tejchman J., Gudehus G,. *Silo-music and silo-quake, experiments and a numerical Cosserat approach*, Powder Technology, 76, 2, 201-212, 1993

[71] Tejchman J., *Numerical study on localized deformation in a Cosserat Continuum, Localisation and Bifurcation Theory for Soils and Rocks*, eds.: R. Chambon, J. Desrues, I. Vardoulakis, Balkema, Rotterdam, 257-275, 1994

[72] Tejchman J., *Silo Quake - Experiments and a Polar Hypoplastic Model*, PARTEC 95, Proc. of the 3rd European Symposium Storage and Flow of Particulate Solids, Nürnberg, 151-163, 1995

[73] Tejchman J., Wu W., *Experimental and Numerical Study of Sand-Steel Interfaces*, Int. J. Num. Anal. Meth. Geomech. 19, 8, 513-537, 1995

[74] Tejchman J., Wu W., *Dynamic Patterning of Shear Bands in a Cosserat Continuum*, Int. Engineer. Mech. Journal ASCE, 123, 2, 123-134, 1997

[75] Tejchman J.: *Shear zones and dynamic effects during silo emptying*, Archives of Civil Engineering, Warsaw, 43, 4, 353–414, 1997

[76] Thornton C., G. Sun., *Axisymmetric compression of 3D polydisperse systems of spheres*, Powders and Grains, eds.: C. Thornton, Balkema, Rotterdam, 129-134, 1993

[77] Uesugi M., *Friction between dry sand and construction*, Dissertation, Tokyo Institute of Technology, 1987

[78] Uesugi M., Kishida H., Tsubakihara Y., *Behaviour of sand particles in sand-steel friction*, Soils and Foundations, 28, 1, 107-118, 1988

[79] Unterreiner P., Vardoulakis I. Boulon M., Sulem, J., *Essential features of a Cosserat continuum in interfacial localisation*, Localisation and Bifurcation Theory for Soils and Rocks, eds.: R. Chambon, J. Desrues, I. Vardoulakis, Balkema, Rotterdam, 141-155, 1994

[80] Vedaie B., Bishara A. G., *Pressures in circular hopper silos under axisymmetric mass flow*, Intern Conf. Silos - Forschung und Praxis, Karlsruhe, SFB 219, 25-55, 1988

[81] Vardoulakis I., *Shear band inclination and shear modulus of sand in biaxial tests*, Int. J. Num. Anal. Met. Geomech. 4, 103-119, 1980

[82] Walker D. M., *A basis for Bunker Design*, Powder Technology, 1, 228-236, 1967

[83] Walters J. K., *A theoretical analysis of stresses with vertical walls*, Chem. Engng. Sci., 28, 13, 1973

[84] Walton O. R., Brown R. L. *Stress calculations for assemblies of inelastic spheres in uniform shear*, Acta Mech., 63, 73-86, 1986

[85] Wu W., *Hypoplasticity model for barotropy and pyknotropy of granular materials*, Veröffentlichungen des Institutes für Boden- und Felsmechanik, Universität Karlsruhe, 129, 1-154, 1992

[86] Yoshimi Y., Kishida T., *Friction between sand and metal surface*, Proc. 10th ICSMFE, 1, 831-834, 1981